DRAFT VERSION MAY 18, 2020
Typeset using LaTeX **twocolumn** style in AASTeX62

Cluster Difference Imaging Photometric Survey (CDIPS) II: A Jupiter-Sized Planet in IC 2602

L. G. BOUMA,[1] R. BRAHM,[2,3,4] J. D. HARTMAN,[1] P. EVANS,[5] G. ZHOU,[6] J. DE LEON,[7] K. G. STASSUN,[8,9] K. A. COLLINS,[6] S. N. QUINN,[6] C. ZIEGLER,[10] J. LIVINGSTON,[7] T. HENNING,[11] A. JORDÁN,[12,4] N. ESPINOZA,[13] W. BHATTI,[1] J. N. WINN,[1] G. Á. BAKOS,[1] G. R. RICKER,[14] R. VANDERSPEK,[14] D. W. LATHAM,[6] S. SEAGER,[15] J. M. JENKINS,[16] AND TSO/SPOC/POC REPRESENTATIVES

[1]*Department of Astrophysical Sciences, Princeton University, 4 Ivy Lane, Princeton, NJ 08540, USA*
[2]*Center of Astro-Engineering UC, Pontificia Universidad Católica de Chile, Av. Vicuña Mackenna 4860, 782-0436 Macul, Santiago, Chile*
[3]*Instituto de Astrofísica, Facultad de Física, Pontificia Universidad Católica de Chile, Av. Vicuña Mackenna 4860, 782-0436 Macul, Santiago, Chile*
[4]*Millennium Institute of Astrophysics, Av. Vicuña Mackenna 4860, 782-0436 Macul, Santiago, Chile*
[5]*El Sauce Observatory, Coquimbo Province, Chile*
[6]*Center for Astrophysics | Harvard & Smithsonian, 60 Garden St, Cambridge, MA 02138, USA*
[7]*Department of Astronomy, University of Tokyo, 7-3-1 Hongo, Bunkyo-ky, Tokyo 113-0033, Japan*
[8]*Vanderbilt University, Department of Physics & Astronomy, 6301 Stevenson Center Lane, Nashville, TN 37235, USA*
[9]*Fisk University, Department of Physics, 1000 17th Avenue N., Nashville, TN 37208, USA*
[10]*Dunlap Institute for Astronomy and Astrophysics, University of Toronto, 50 St. George Street, Toronto, Ontario M5S 3H4, Canada*
[11]*Max-Planck-Institut für Astronomie, Königstuhl 17, 69117 Heidelberg, Germany*
[12]*Facultad de Ingeniería y Ciencias, Universidad Adolfo Ibáñez, Av. Diagonal las Torres 2640, Peñalolén, Santiago, Chile*
[13]*Space Telescope Science Institute, 3700 San Martin Drive, Baltimore, MD 21218, USA*
[14]*Department of Physics and Kavli Institute for Astrophysics and Space Research, Massachusetts Institute of Technology, Cambridge, MA 02139, USA*
[15]*Department of Earth, Atmospheric, and Planetary Sciences, Massachusetts Institute of Technology, Cambridge, MA 02139, USA*
[16]*NASA Ames Research Center, Moffett Field, CA 94035, USA*

(Received May 18, 2020; Revised —; Accepted —)

Submitted to AAS journals.

ABSTRACT

We report the discovery of the transiting planet TOI 837.01, a warm Jupiter-sized planet ($R_p = 10.XX\,R_\oplus$, $P = 8.YY$ d), with mass less than X.XX $M_{\rm Jup}$. TOI837.01 orbits a V=10.6, T=9.9 G-dwarf in IC 2602 (the "Southern Pleiades") and is therefore 50 million years old. We characterize the system using data from the NASA *Transiting Exoplanet Survey Satellite* (TESS), the ESA Gaia mission, ground-based photometry, and spectroscopy from CTIO1.5/CHIRON, XXX/FEROS, and AAT/Veloce. TOI 837.01 joins the growing ranks of adolescent exoplanets orbiting bright host stars, and is amenable for studies of planetary atmospheric and orbital evolution.

Keywords: Exoplanets (XXX), Exoplanet evolution (491), Stellar ages (1581), Young star clusters (XXX)

1. INTRODUCTION

Recently, young planets have been hype.
TESS (Ricker et al. 2015).
Section 2 Section 3 Section 4 Section 5 Section 6.

2. THE DATA

2.1. *TESS Photometry*

TOI 837 (GAIA DR2 5251470948229949568) was observed by the TESS spacecraft from X to Y in two-minute cadence mode. The star was designated TIC 460205581 in the TESS Input Catalog (Stassun et al. 2018, 2019). The pixel data for an 11×11 array surrounding TOI 837 were averaged into 2-minute stacks by the onboard computer. Each 2048×2048 image from the CCD was also averaged into 30-minute stacks, and saved as a "full frame image" (FFI).

The pixel data for an The 2-minute stacks for TOI 837 were reduced to lightcurves by the Science Processing Operations Center (SPOC) at NASA Ames (Jenkins et al. 2016). We mainly used the Presearch Data Conditioning (PDC) lightcurve. The PDC lightcurve aperture used pixels chosen to maximize the SNR of the total flux of the target (**?**). Non-astrophysical variability was removed by fitting out trends common to many stars (**??**).

As an independent check on the 2-minute SPOC lightcurve, we examined the lightcurve based upon 30-minute image

Corresponding author: L. G. Bouma
luke@astro.princeton.edu

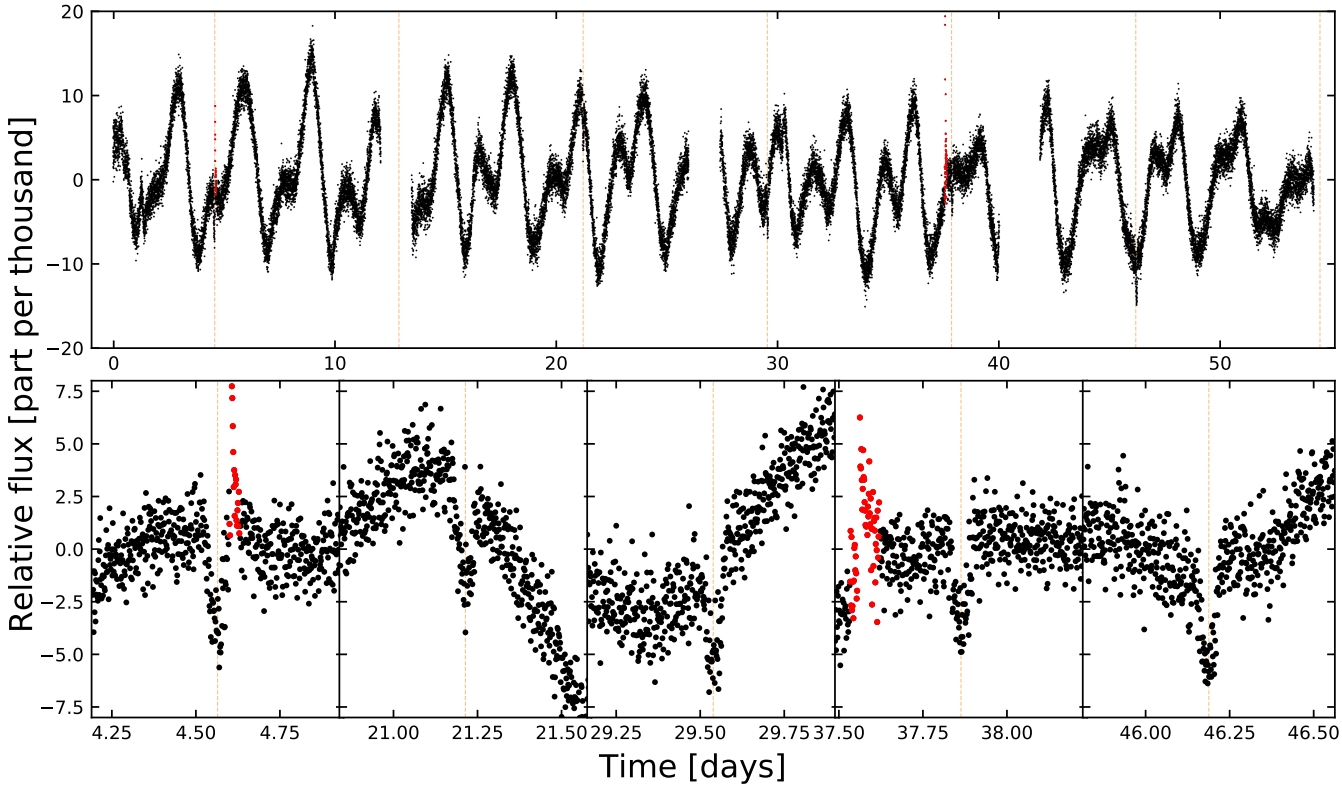

Figure 1. TESS lightcurve of TOI 837 (Sectors 10 and 11). *Top*: PDCSAP mean-subtracted relative flux at 2-minute sampling. Spot-induced stellar variability is the dominant signal. Dashed lines show the five transits observed by TESS. *Bottom*: Zoomed windows of individual transits. Red points show manually identified stellar flares.

stacks which was produced as part of the Cluster Difference Imaging Photometric Survey (CDIPS; Bouma et al. 2019). Our CDIPS lightcurve of choice used a circular aperture with radius 1 pixel.

Figure 1.

2.2. *Ground-based Time-Series Photometry*

2.3. *Imaging*

2.4. *Spectroscopy*

2.4.1. *CHIRON*

9 spectra with CTIO1.5/CHIRON, from January 28 through March 14, 2020. 6 were usable.

2.4.2. *FEROS*

N spectra with XXX/FEROS

2.4.3. *Veloce*

M spectra with AAT/Veloce.

2.5. *Astrometry*

3. THE STAR

3.1. *The Cluster*

IC 2602 canonically has an age of 30 ± 20 Myr (CITE: Van Leeuwen 2009). Or logage between 7.533 and 7.563 (Bossini et al. 2019).

Or Li age of 40-50Myr (David+19, comparison with other Li stars).

Reported mean metallicity values [Fe/H] for the cluster range between slightly super-solar (0.04 ± 0.01, Baratella et al. 2020) and slightly sub-solar (-0.02 ± 0.02, Netopil et al. 2016).

IC 2602 is supervirial, in the sense that the observed stellar velocity dispersion is larger than the value expected if it were in virial equilibrium by about a factor of two (Bravi et al. 2018).

3.2. *Cluster Membership*

TOI 837 has been reported as a member of IC 2602 by multiple independent investigators (Kharchenko et al. 2013; Cantat-Gaudin et al. 2018).

The Gaia kinematics are good; gamma velocity is correct; Li (FEROS + Veloce) is strong; the rotation period and vsini agree with sub-Pleiades age expected for an IC 2602 member.

3.2.1. *HR Diagram*

Figure 3 shows a Hertzsprung-Russell diagram of TOI 837 in reference to the broader IC 2602 cluster, as well as its neighborhood. Cluster members were identified by Cantat-Gaudin et al. (2018) using using Gaia-DR2 positions, proper motions, and parallaxes. We included candidate members with formal membership probability exceeding 10%. Save

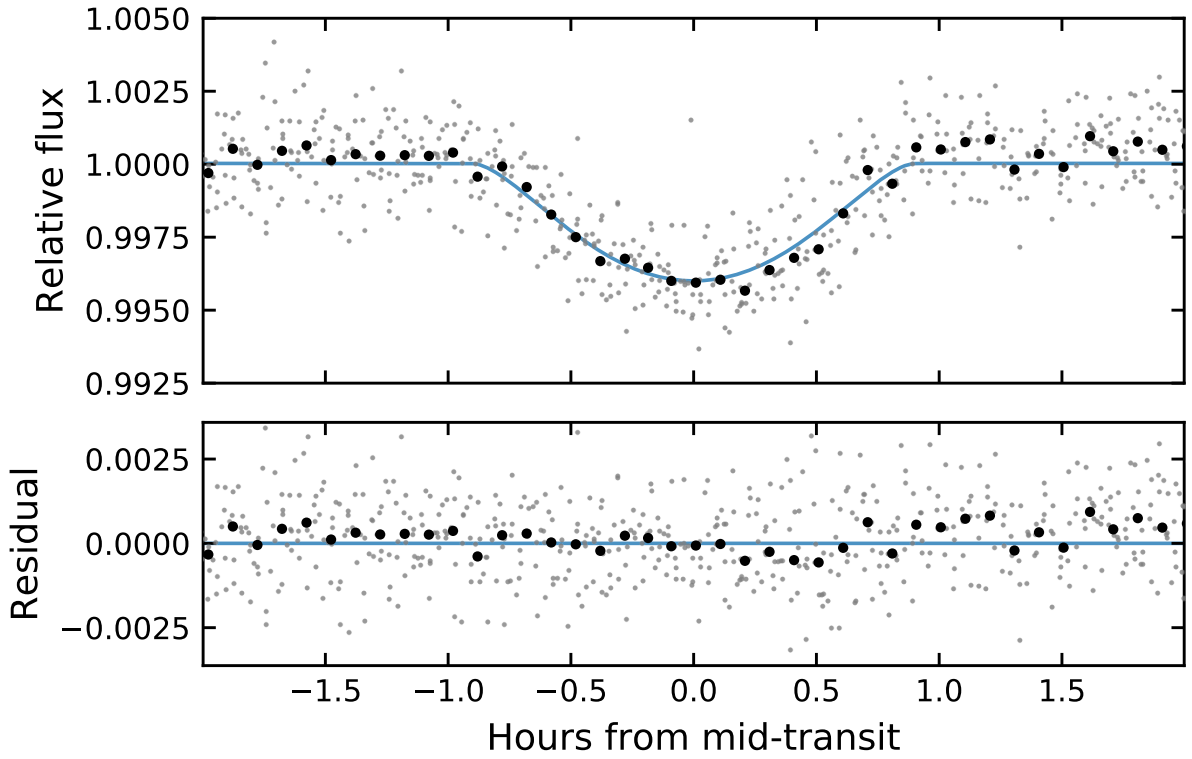

Figure 2. Phase-folded transit of TOI 837.01. Gray points are 2-minute PDCSAP flux measurements, detrended with a 0.3-day robust Huber spline (see Section 2.1). Black points are binned to approximately 1 point per 6 minutes. The blue line shows the transit model corresponding to the median transit parameters (Table 2).

for a few low-mass outliers, most members appear to be young and coeval.

TOI 837 is in its expected position relative to the other members along the cluster isochrone. This photometrically limits the presence of binary companions in the TOI 837 system, to a magnitude difference of perhaps half the brightness of the target star.

Figure 3 also suggests that the membership census of IC 2602 is incomplete. We defined the reference "neighborhood" as the group of at most 10^4 randomly selected non-member stars within 5 standard deviations of the mean IC 2602 right ascension, declination, and parallax. We queried Gaia DR2 for these stars using `astroquery` (Ginsburg et al. 2018). Many low-mass stars appear above the main sequence, even though they were not identified as 5-dimensional kinematic members through the unsupervised **?** membership assignment process.

3.2.2. *Position and Kinematics*

We examine the six-dimensional positions and kinematics in greater depth in Figure 4. The "neighborhood" is defined here identically to as in Figure 3. The axes limits for the right ascension, declination, and parallax dimensions are as in the Gaia archive query. The axes limits for the proper motion and radial velocity dimensions are set at the 25$^{\rm th}$ and 75$^{\rm th}$ percentiles, in order to give a sense of the population's distribution, while excluding outlying points. The radial velocities suffer the greatest incompleteness due to the current $G \approx 12$ magnitude limit of the Gaia-DR2 data processing.

Figure 4 provides strong evidence *(i)* for the existence of the IC 2602 open cluster and *(ii)* for the membership of TOI 837 within IC 2602. The only dimension that could perhaps lead to some worry is the parallax, as TOI 837 is one of the closest IC 2602 members reported by Cantat-Gaudin et al. (2018). Fortunately, there are independent means of verifying stellar youth.

3.2.3. *Rotation*

TESS photometric rotation period = 3.5days ish.
vsini = 17.48 $\pm$ 0.15 (CHIRON).
The two agree.
For comparison, gyrochrones would predict X.XX.
This implies sub-Pleiades age expected for an IC 2602 member.

3.2.4. *Lithium*

Rafael's co-added FEROS spectra gave a Li doublet equivalent width of 154 milliangstrom (see attached).

As a reminder, Teff=6100K (TICv8). Or Teff = 5946 $\pm$ 39 (CHIRON). Rafael, if you have a better determination of Teff, it would be helpful! SpType is early-G, late-F from your quicklook spectral typing earlier.

Relevant colors are V-K = 1.7, V-I = V-T = 0.7
Summarizing relevant lithium facts:

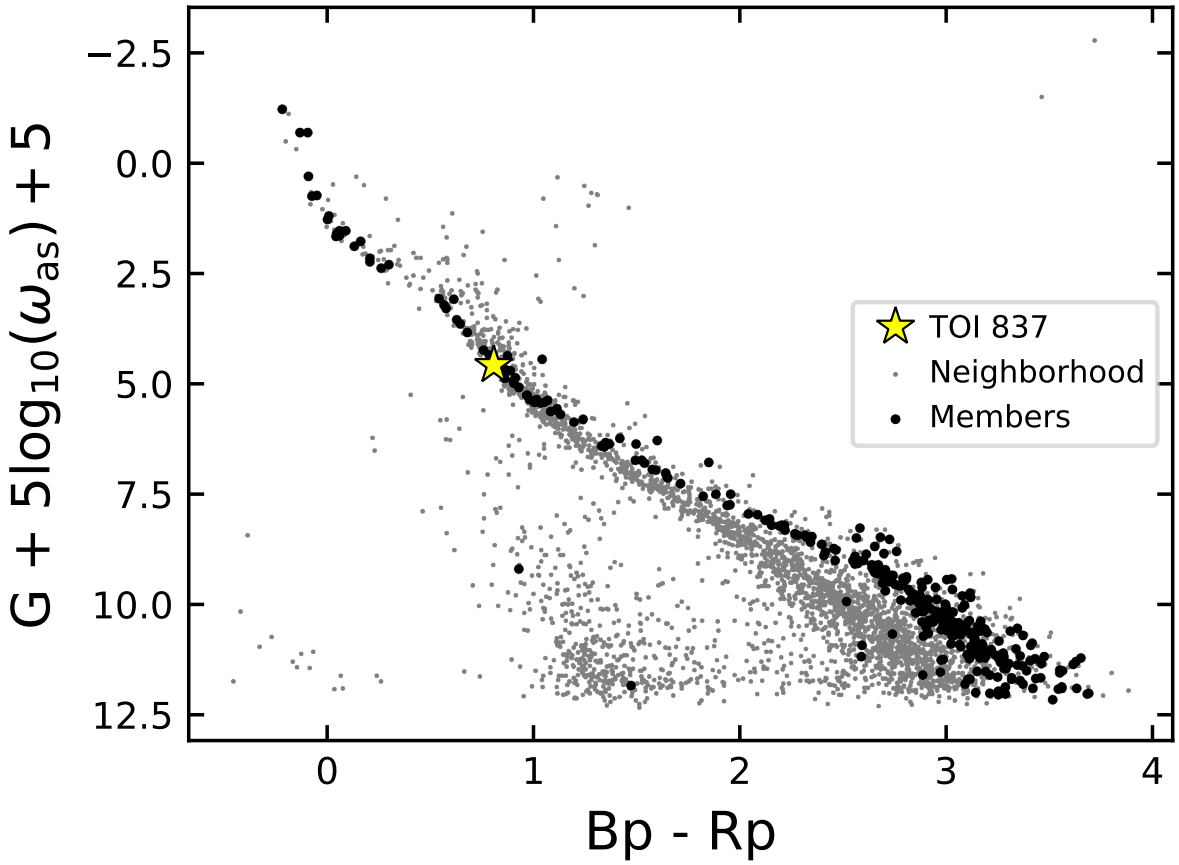

Figure 3. Hertzsprung-Russell diagram of TOI 837 and members of IC 2602. Members (black circles) were identified by Cantat-Gaudin et al. (2018). Gray circles are non-member stars within 5 standard deviations of the mean IC 2602 right ascension, declination, and parallax. *G* denotes Gaia broadband magnitudes, *Bp* Gaia blue, *Rp* Gaia red, and ω_{as} the parallax in arcseconds.

Lithium depletion for a star of TOI-837's spectral type happens over timescales >100 Myr (Soderblom+2013). This is because the convective envelopes are very shallow, so they don't cycle material down to the >3e6 K core until much later.

Nonetheless, comparison of early-G field stars to e.g., 600 Myr old Hyads shows that the depletion does happen over gigayear timescales (Berger+2018, fig 7).

Comparing to the Li EWs measured by Berger+2018 (their Fig 5), TOI-837 is consistent with being younger than almost all CKS planet-hosting field stars.

The TOI-837 Li EW measured here (150 milliangstrom) is consistent with what's seen for stars of similar colors in <100 Myr old moving groups (Elliott+2016, Fig 11 – attached). This is sensible, because IC 2602 is supposed to be 50 Myr old.

3.2.5. *Literature Membership*

The membership of TOI 837 in IC 2602 was noted by Oh et al. (2017), in what they dubbed "Group 5". Analyzing the clusters of Oh et al. (2017), **?** fitted the Gaia, 2MASS, and WISE photometry with MIST isochrones, and reported stellar masses, radii, metallicities, ages, distances, and extinction for 9754 stars, including TOI 837.

TOI 837 was also listed as a member of "Theia 92" by **?**. These authors identified 999 candidate cluster members, and reported a cluster isochrone age $\log t = 7.55$ with uncertainty ≈ 0.15 dex.

3.3. *Stellar Parameters*

3.3.1. *Physical*

(Lstar, Rstar, Teff, Age and Mstar)

From CHIRON spectra, my current best guess spectroscopic parameters are as follows. Teff = 5946 +/- 39 logg = 4.48 +/- 0.03 feh = -0.065 +/- 0.035 vsini = 17.48 +/- 0.15

Figure 5. The SED fit, looking really good with rchi2 = 1.6:

The fit parameters are: Av = 0.20 +/- 0.03 Fbol = 1.967 +/- 0.046 e-9 erg/s/cm2 Rstar = 1.049 +/- 0.019 Rsun

From the spectroscopic logg and the above Rstar, we get an independent mass estimate of Mstar = 1.21 +/- 0.10 Msun At face value, the mass seems a bit high for the radius, but I'm guessing that just means the spectroscopic logg is a bit too high.

Astrometric information—The RUWE (CITE, CITE) for TOI 837 is 1.02, indicative that there are no obviously present astometric companions.

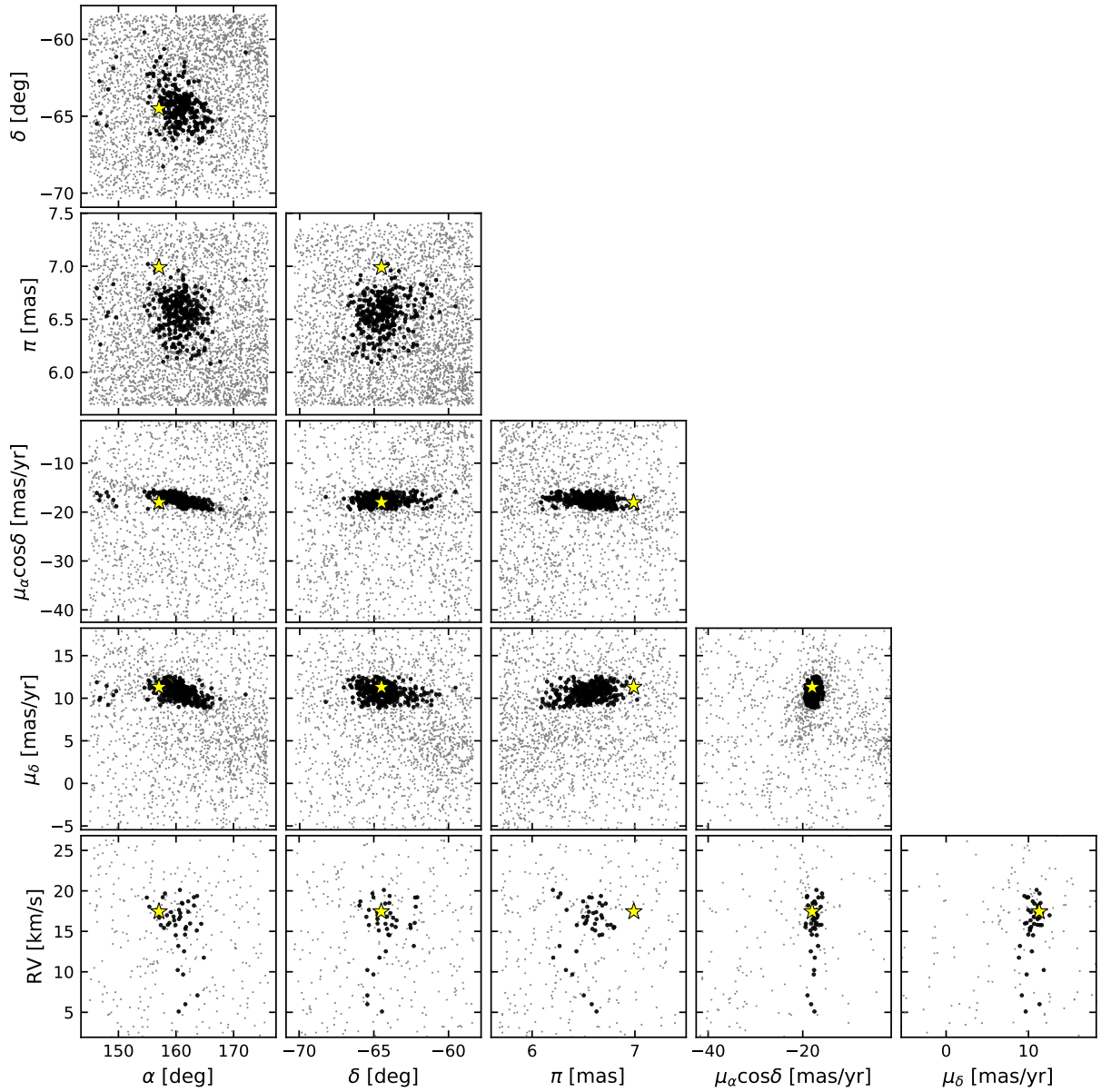

Figure 4. Positions and kinematics of TOI 837 (star), IC 2602 members (black circles), and stars in the neighborhood (gray circles). Members were identified by Cantat-Gaudin et al. (2018). α denotes right ascension, δ declination, π parallax, $\mu_{\rm delta}$ and μ_α proper motion in each equatorial direction, and RV radial velocity reported by Gaia-DR2. The RVs are for unblended spectra of bright stars ($G \lesssim 12$). The proper motion projection (μ_δ vs. $\mu_\alpha \cos\delta$) highlights the membership selection function.

3.3.2. *Rotation*

Stellar vsini Stellar rotation

3.4. *RVs*

I don't strongly expect the Veloce RVs or the FEROS ones to lead to a mass measurement. The reason is that with vsini=17km/s, and 2% rotation amplitude signal, we expect an RV RMS of 300m/s at the Prot=3.5 day rotation period (vsini*rotation amplitude). This is probably larger than the expected planet signal (100m/s, 8 days).

4. THE PLANET

4.1. *Transit Fitting*

Simultaneous dip plus rotation period (GP) fit. Use celerite plus PyMC3/exoplanet. Mention FPP?

4.2. *Validation of TOI 837.01*

Exclude possibilities: "The transits are blended from a background, unassociated eclipsing binary system or transiting exoplanet: We take the same approach outlined in Vanderburg et al. (2019). In short, if the transits are a blend from the background system, the true radius ratio is constrained by the ratio of the ingress time (T12) to the..."

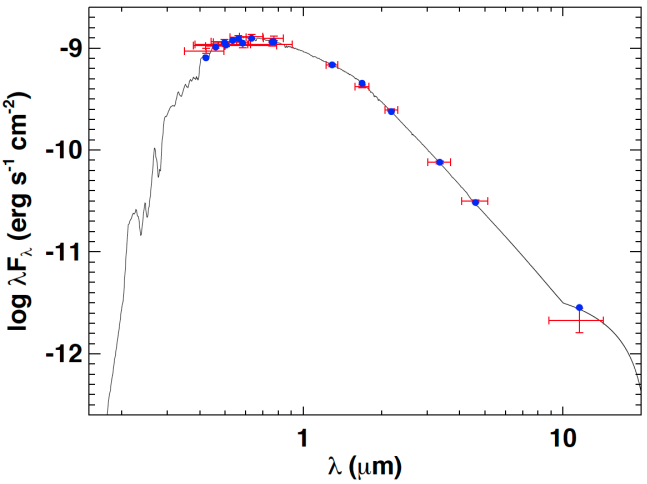

Figure 5. Spectral energy distribution of TOI 837 from archival photometry. Keivan: please describe, and if possible, send me the data (photometry + the atmosphere model) used to generate the plot so I can regenerate it in a consistent style with the rest of the paper

Given its galactic latitude of only −6°, it is not surprising that the field of TOI 837 is crowded. A number of possible false-positive explanations, including the usual neighboring, background, and hierarchical eclipsing binary scenarios, must therefore be considered.

For these scenarios to be viable, the flux from TOI 837 and the true eclipsing binary host would blend together, reducing the "true" eclipse depth $\delta_{\rm true}$ to produce the observed depth $\delta_{\rm obs}$:

$$\delta_{\rm obs} = \delta_{\rm true} \frac{F_{\rm neighbor}}{F_{\rm total}}, \quad (1)$$

where the total flux and the flux from the neighbor are labelled as such. The requirement that the true eclipse depth is less than one translates to a bound on the faintest possible blended companion stars:

$$\Delta m < -\frac{5}{2} \log_{10} \delta_{\rm obs}. \quad (2)$$

For TOI 837 ($T = 9.93$), this implies that any star invoked to explain the transit depth must be brighter than $T = 15.92$.

There's also

$$\Delta m < -\frac{5}{2} \log_{10}(\delta_{\rm obs} t_{12}^2 / t_{13}^2). \quad (3)$$

4.2.1. *Visual Binarity*

Figure 6 shows the scene. In the upper panels, the pixels used to measure the background level in the SPOC lightcurve are indicated with 'X' hatching, and the pixels used in the final lightcurve aperture are shown with '/' hatching.

Stars brighter than $T = 16$, as queried from the Gaia DR2 source catalog, are shown with orange circles. The relevant stars for a blend analysis are as follows.

- TOI 837 = TIC 460205581 (T=9.9). The target star.

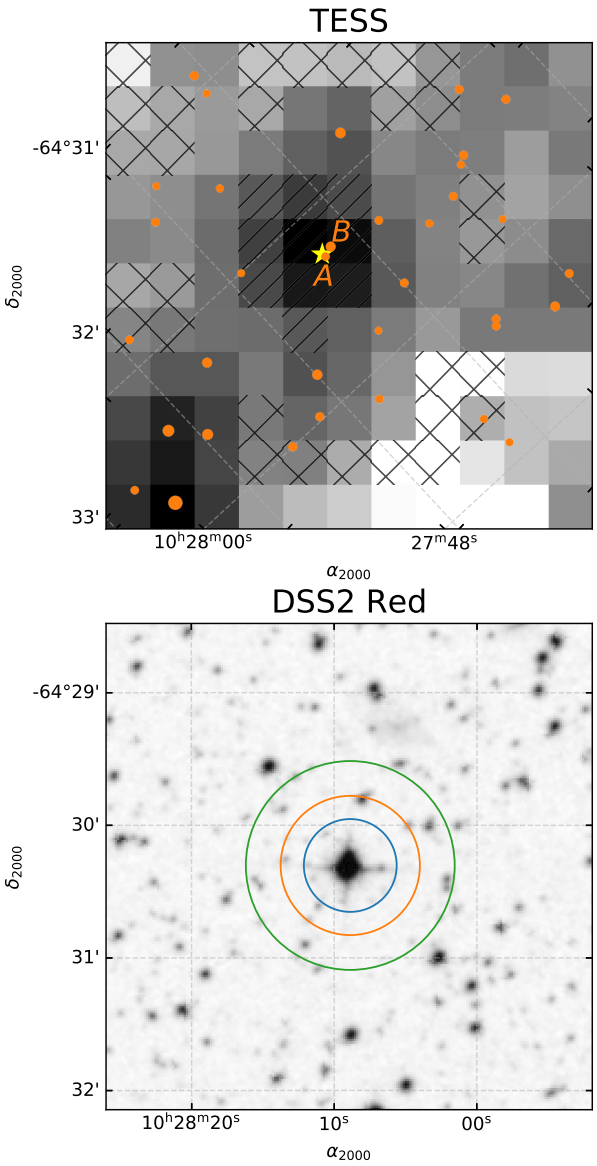

Figure 6. Scene used for blend analysis. *Top:* Mean TESS image of TOI 837 over Sector 10, with a logarithmic grayscale. The yellow star is the position of TOI 837. Orange circles are neighboring stars with $T < 16$, scaled such that brighter stars are larger. The X and / hatches show the apertures used to measure the background and target star flux, respectively. Dashed lines of constant declination and right ascension are shown. *Bottom:* Digitized Sky Survey *R*-band image of the same field, with a linear grayscale. The circles show apertures of radii 1, 1.5, and 2.25 pixels used in our blend analysis (Section 4.2). Two stars of interest are "Star A" and "Star B", which were eventually excluded as being possible sources of the transits.

- Star A = TIC 847769574 (T=14.6). 2.3" west. Proper motions and parallax imply it is comoving with TOI 837, though with a physical separation of 6.6 ± 0.1 pc, it may not be bound.

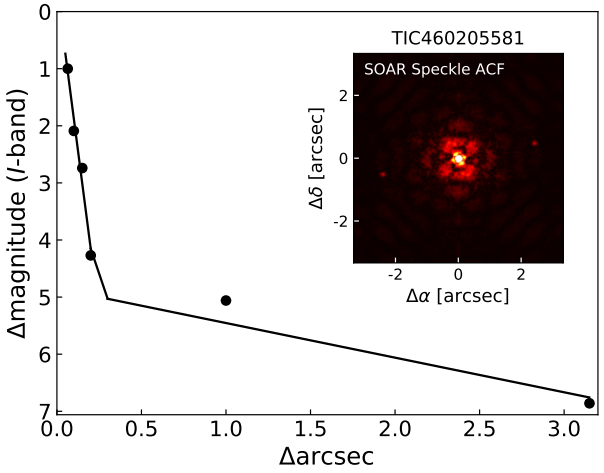

Figure 7. SOAR HRCam contrast limits derived from point-source injection-recovery experiments. Star A (ΔT = 4.7, ρ = 2.3" west) is detected in the autocorrelation function, in addition to being a resolved Gaia source. It is co-moving with TOI 837, and its parallax and on-sky position imply that it is physically separated from TOI 837 by 6.6 ± 0.1 pc.

- Star B = TIC 460205587 (T=13.1). 5.4" north. This is a giant background star.

An additional source, TIC 847769581, is 4.9" from the target, but too faint (T=18.8) to be the source of the observed transit signal.

The Gaia DR2 data for Star A seems somewhat poorly behaved. While Star A has G = 15.1, and Bp = 14.9, no Rp magnitude is reported. Correspondingly, no RUWE value is available (CITE). The astrometric reduced χ^2 ($\chi^2/(N-5)$, for N the number of good astrometric observations) seems rather poor, at 8.6. We suspect that the photometric failure to produce an Rp magnitude, as well as the poor astrometric fit, are likely due to blending with TOI 837.

At the angular resolution of the TESS data, if either Star A or Star B were eclipsing binaries, they could be the sources of the transit signal. Coincidence stellar sources below the resolution limit of Gaia are also a concern (CITE). To rule out these possibilities, we took a number of approaches.

4.2.2. *High-resolution imaging*

We imaged the system using SOAR-HRCam. **Carl: please describe**. Figure 7. Ziegler et al. (2020)

4.2.3. *TESS analysis*

We examined the CDIPS FFI lightcurves of the target, which are available on MAST (Bouma et al. 2019). Three lightcurves are available, based on photometric apertures with a radius of 1, 1.5, or 2.5 pixels. In the raw difference-image light-curves, as well as the PCA-detrended light-curves, dips of depth ≈0.35% are visible, and their properties do not significantly vary with aperture size. Within ≈ 20", the dips are consistent with originating from the target star.

4.2.4. *Seeing-limited time-series photometry*

left off here Co-author P. Evans obtained a total transit that showed that, within 1.5", the transit comes from TOI 837. We can be even more certain with a pixel-level analysis. This 2.1 arcsec neighbor is also a mid to late M dwarf, and bound given the Gaia parallax + proper motion. The transit duration is rather long for the signal to come from the M dwarf, rather than the G dwarf. I think the state of photometric followup could be improved (there is only one good total transit), but I think over this month and next we can pull another few partials.

A total eclipse of Ziegler's faint companion would produce a 1.4% dip. A 30% eclipse, more plausible for a NEB scenario, would produce dips at exactly the right depth (0.4%).

dmag = 4.7, transit depth is 0.4%. This dmag converts to a flux fraction of 0.0132. A 30% eclipse on T1 could therefore nominally explain the TESS data.

However in the aperture from this green r=2px green LC, say 90% of the flux from T1 is excluded. The eclipse on T1 would therefore need to be much deeper – in fact, over 100%. This argument holds as long as at least 70% of the flux from T1 is excluded, so I think we're likely in the clear.

4.2.5. *Summary*

Possible false-positive scenarios are as follows.

- *Neighboring blends*.
- *Hierarchical blends*. Limited by i) FEROS + Veloce RVs, and ii) the star being nicely on the cluster HR diagram. Any extra hidden close-in binary stars would need to be very low-mass M dwarfs, and then the transit duration again helps.
- *Background blends*. Archival SERC-J and AAO-SES plates are available for the TOI 837 field[1]. These plates were acquired in 1982 and 1992, respectively. For high proper motion stars archival imagery can be used to detect slowly moving background stars that might be an astrophysical false-positive source (*e.g.*, Huang et al. 2018). However TOI 837 has only moved $\approx 0.7''$ between 1982 and present, in comparison to the $\approx 2.0''$ FWHM of the target on the plates. We therefore cannot resolve it with great confidence from background sources not already resolved through more modern imaging.

4.3. *Additional Companions*

None of the extra dips in the PDCSAP light-curve (e.g., "up-down" spikes at BTJD 1572 and 1601) seem likely to be planetary We checked that i) they were not present in the SAPFLUX light-curves, and ii) that they were not present in the CDIPS light-curves (either raw, or PCA-detrended).

To make this quantitative, we did injection-recovery.

[1] https://archive.stsci.edu/cgi-bin/dss_form

5. DISCUSSION

In context,...

6. CONCLUSIONS

The authors thank... We also thank the Heising-Simons Foundation for their generous support of this work. The Digitized Sky Survey was produced at the Space Telescope Science Institute under U.S. Government grant NAG W-2166. Figure 6 is based on photographic data obtained using the Oschin Schmidt Telescope on Palomar Mountain. This research made use of the Exoplanet Follow-up Observation Program website, which is operated by the California Institute of Technology, under contract with the National Aeronautics and Space Administration under the Exoplanet Exploration Program.

Software: `astrobase` (Bhatti et al. 2018), `astropy` (Astropy Collaboration et al. 2018), `astroquery` (Ginsburg et al. 2018), `cdips-pipeline` (Bhatti et al. 2019) `corner` (Foreman-Mackey 2016), `exoplanet` (Agol et al. 2019) `exoplanet` (Foreman-Mackey et al. 2020), and its dependencies (Agol et al. 2019; Kipping 2013; Luger et al. 2019; Theano Development Team 2016). `IPython` (Pérez & Granger 2007), `lightkurve` (Lightkurve Collaboration et al. 2018), `matplotlib` (Hunter 2007), `MESA` (Paxton et al. 2011, 2013, 2015) `numpy` (Walt et al. 2011), `pandas` (McKinney 2010), `pyGAM` (Servén et al. 2018), `PyMC3` (Salvatier et al. 2016), `scipy` (Jones et al. 2001). `tesscut` (Brasseur et al. 2019), `wotan` (Hippke et al. 2019).

Facilities: *Astrometry*: Gaia (Gaia Collaboration et al. 2016, 2018). *Imaging*: Second Generation Digitized Sky Survey, Keck:II (NIRC2; www2.keck.hawaii.edu/inst/nirc2). *Spectroscopy*: Keck:I (HIRES; Vogt et al. 1994). *Photometry*: TESS (Ricker et al. 2015).

Table 1. Model Comparison.

Description	N_s	N_ℓ	N_{data}	N_{param}	χ^2	χ^2_{red}	BIC	ΔBIC
Favored	2	2	2585	17	3230.2	1.258	3363.7	0.0
Weakly favored	3	3	2585	21	3203.4	1.249	3368.4	4.7
—	3	2	2585	19	3222.9	1.256	3372.2	8.4
Disfavored	2	3	2585	19	3244.9	1.265	3394.2	30.4
—	2	1	2585	15	3410.6	1.327	3528.5	164.7
—	3	1	2585	17	3396.4	1.323	3530.0	166.3
—	1	2	2585	15	4158.6	1.618	4276.4	912.7
—	1	3	2585	17	4147.4	1.615	4281.0	917.2
—	1	1	2585	13	4313.5	1.677	4415.6	1051.9

NOTE— N_s and N_ℓ are the number of harmonics at the short and long periods, respectively. N_{data} is the number of fitted flux measurements. N_{param} is the number of free parameters in the model. The Bayesian information criterion (BIC) and the difference from the maximum ΔBIC are also listed.

Table 2. Best-fit model priors and posteriors.

Param.	Unit	Prior	Median	Mean	Std. Dev.	3%	97%
P_s	d	$\mathcal{N}(8.3247;0.0050)$	8.3248321	8.3248295	0.0003356	8.3242288	8.3254817
$t_s^{(1)}$	d	$\mathcal{N}(1574.273800;0.0050)$	1574.2727299	1574.2727323	0.0010770	1574.2707084	1574.2747189
$\log R_p/R_\star$	–	$\log\mathcal{U}(0.01;1.00)$	-2.43072	-2.236	0.55106	-2.74890	-0.99823
b	–	$\mathcal{U}(0;1+R_p/R_\star)$	0.9729	1.0221	0.1533	0.9165	1.2972
u_1	–	$\mathcal{U}(0.186;0.486)^{(2)}$	0.335	0.335	0.088	0.187	0.469
u_2	–	$\mathcal{U}(0.075;0.375)^{(2)}$	0.229	0.227	0.086	0.093	0.374
Mean	–	$\mathcal{U}(0.99;1.01)$	1.000028	1.000028	0.000006	1.000016	1.000039
$R_\star$	$R_\odot$	$\mathcal{T}(1.05;0.06)$	1.05	1.05	0.06	0.94	1.16
$\log g$	cgs	$\mathcal{N}(4.48;0.09)$	4.46	4.46	0.08	4.32	4.61
$R_p/R_\star$	–	–	0.09	0.13	0.14	0.06	0.37
$\rho_\star$	g cm^{-3}	–	1.42	1.44	0.28	0.97	1.97
R_p	R_{Jup}	–	0.90	1.38	1.44	0.58	3.87
$a/R_\star$	–	–	17.33	17.35	1.11	15.28	19.33
$\cos i$	–	–	0.06	0.06	0.01	0.05	0.08
T_{14}	hr	–	1.79	1.79	0.05	1.68	1.87
T_{13}	hr	–	0.27	0.28	0.12	0.01	NaN

Note: T_{13} is ill-defined for a grazing transit.

(1) To convert mean TESS mid-transit time from BTJD to BJD_{TDB}, add 2,457,000.

(2) Assuming an informative quadratic limb-darkening prior with uniform values about those given for the appropriate T_{eff} and $\log g$ from Claret (2017).

REFERENCES

Agol, E., Luger, R., & Foreman-Mackey, D. 2019, arXiv e-prints, 1908.03222

Astropy Collaboration, Price-Whelan, A. M., Sipőcz, B. M., et al. 2018, AJ, 156, 123

Baratella, M., D'Orazi, V., Carraro, G., et al. 2020, Astronomy and Astrophysics, 634, A34

Bhatti, W., Bouma, L., & Yee, S. 2019, `cdips-pipeline v0.1.0`, https://doi.org/10.5281/zenodo.3370324

Bhatti, W., Bouma, L. G., & Wallace, J. 2018, `astrobase`, https://doi.org/10.5281/zenodo.1469822

Bossini, D., Vallenari, A., Bragaglia, A., et al. 2019, Astronomy and Astrophysics, 623, A108

Bouma, L. G., Hartman, J. D., Bhatti, W., Winn, J. N., & Bakos, G. Á. 2019, ApJS, 245, 13

Brasseur, C. E., Phillip, C., Fleming, S. W., Mullally, S. E., & White, R. L. 2019, Astrophysics Source Code Library, ascl:1905.007

Bravi, L., Zari, E., Sacco, G. G., et al. 2018, Astronomy and Astrophysics, 615, A37

Cantat-Gaudin, T., Jordi, C., Vallenari, A., et al. 2018, Astronomy & Astrophysics, 618, A93

Claret, A. 2017, Astronomy & Astrophysics, 600, A30, arXiv: 1804.10295

Foreman-Mackey, D. 2016, The Journal of Open Source Software, 24

Foreman-Mackey, D., Czekala, I., Luger, R., et al. 2020, exoplanet-dev/exoplanet v0.2.6

Gaia Collaboration, Prusti, T., de Bruijne, J. H. J., et al. 2016, A&A, 595, A1

Gaia Collaboration, Brown, A. G. A., Vallenari, A., et al. 2018, A&A, 616, A1

Ginsburg, A., Sipocz, B., Madhura Parikh, et al. 2018, Astropy/Astroquery: V0.3.7 Release

Hippke, M., David, T. J., Mulders, G. D., & Heller, R. 2019, arXiv:1906.00966 [astro-ph], arXiv: 1906.00966

Huang, C. X., Burt, J., Vanderburg, A., et al. 2018, ApJ, 868, L39

Hunter, J. D. 2007, Computing in Science & Engineering, 9, 90

Jenkins, J. M., Twicken, J. D., McCauliff, S., et al. 2016, Software and Cyberinfrastructure for Astronomy IV, 9913, 99133E

Jones, E., Oliphant, T., Peterson, P., et al. 2001, Open source scientific tools for Python

Kharchenko, N. V., Piskunov, A. E., Schilbach, E., Röser, S., & Scholz, R.-D. 2013, Astronomy and Astrophysics, 558, A53

Kipping, D. M. 2013, MNRAS, 435, 2152

Lightkurve Collaboration, Cardoso, J. V. d. M., Hedges, C., et al. 2018, Lightkurve: Kepler and TESS time series analysis in Python, Astrophysics Source Code Library, ascl:1812.013

Luger, R., Agol, E., Foreman-Mackey, D., et al. 2019, AJ, 157, 64

McKinney, W. 2010, in Proceedings of the 9th Python in Science Conference, ed. S. van der Walt & J. Millman, 51

Netopil, M., Paunzen, E., Heiter, U., & Soubiran, C. 2016, Astronomy and Astrophysics, 585, A150

Oh, S., Price-Whelan, A. M., Hogg, D. W., Morton, T. D., & Spergel, D. N. 2017, The Astronomical Journal, 153, 257

Paxton, B., Bildsten, L., Dotter, A., et al. 2011, ApJS, 192, 3

Paxton, B., Cantiello, M., Arras, P., et al. 2013, ApJS, 208, 4

Paxton, B., Marchant, P., Schwab, J., et al. 2015, ApJS, 220, 15

Pérez, F., & Granger, B. E. 2007, Computing in Science and Engineering, 9, 21

Ricker, G. R., Winn, J. N., Vanderspek, R., et al. 2015, Journal of Astronomical Telescopes, Instruments, and Systems, 1, 014003

Salvatier, J., Wieckiâ, T. V., & Fonnesbeck, C. 2016, PyMC3: Python probabilistic programming framework

Servén, D., Brummitt, C., & Abedi, H. 2018, dswah/pyGAM: v0.8.0

Stassun, K. G., Oelkers, R. J., Pepper, J., et al. 2018, AJ, 156, 102

Stassun, K. G., Oelkers, R. J., Paegert, M., et al. 2019, arXiv:1905.10694 [astro-ph], arXiv: 1905.10694

Theano Development Team. 2016, arXiv e-prints, abs/1605.02688

Vogt, S. S., Allen, S. L., Bigelow, B. C., et al. 1994, SPIE Conference Series, ed. D. L. Crawford & E. R. Craine, Vol. 2198

Walt, S. v. d., Colbert, S. C., & Varoquaux, G. 2011, Computing in Science & Engineering, 13, 22

Ziegler, C., Tokovinin, A., Briceño, C., et al. 2020, AJ, 159, 19